TriDurLE

National Center for Transportation Infrastructure Durability & Life-Extension

Project ID: 2020-MST-03

PERFORMANCE OF WICKING GEOTEXTILE (H2RI) TO MITIGATE PAVEMENT PUMPING

PHASE 2

Final Report

By

Javad Galinmoghadam, M.Sc.
Graduate Research Assistant
Missouri University of Science and Technology

Xiong Zhang, Ph.D., P.E.
Professor of Civil Engineering
Missouri University of Science and Technology

for

National University Transportation Center TriDurLE
Department of Civil & Environmental Engineering
405 Spokane Street PO Box 642910
Washington State University Pullman, WA 99164-2910

November 25, 2022

Acknowledgements

The author wishes to express their appreciation to the Missouri Department of Transportation (MODOT) for sponsoring this research project and TENCATE GEOSYNTHETICS (North America) for donating the wicking geotextile needed for this research. The research team would like to avail this opportunity to wholeheartedly thank Mr. John P. Donahue, Construction and Materials Liaison Engineer, Mr. Bill Stone, former Research Administrator, and Christopher Graham, Resident Engineer of MODOT for their great help and support during the process. Without their help, this study would have been impossible. Many graduate students in the Geotechnical Group at Missouri S&T helped the fieldwork including Chuang Lin, Yipeng Guo, Beshoy Riad, Shanmei Li, Donggen Chen, Anyou Zhu, and Xinxing Zhou. Their help during the process is highly appreciated as well.

Disclaimer

This document is disseminated under the sponsorship of the Missouri Department of Transportation in the interest of information exchange. The Missouri Government assumes no liability for the use of the information contained in this document. The Missouri Government does not endorse products or manufacturers. Trademarks or manufacturers' names appear in this report only because they are considered essential to the objective of the document.

Opinions and conclusions expressed or implied in the report are those of the author(s). They are not necessarily those of the funding agencies. This report does not constitute a standard, specification, or regulation.

Copyright

Table of Contents

List of Figures

Abstract

Pumping is one of the major factors contributing to pavement failures, which reduces the pavement life, affects road safety, and increases maintenance costs. Existing methods that are used as drainage systems can drain gravitational (free) water under saturated conditions but not the capillary water under an unsaturated condition. The objective of this study is to explore and identify the feasibility of using a new wicking geotextile for pumping mitigation in pavement shoulder via laboratory tests and field test section monitoring. Results obtained from monitoring the field test section for more than three years verified the effectiveness of using wicking geotextile to reduce water content, especially where the pavement is prone to pumping damage. As a result, the generation of positive pore water pressure is delayed if not completely prevented. In this way, one of the requirements of pavement pumping is eliminated.

Executive Summary

A new type of wicking geotextile was used to mitigate pumping in pavement systems. This type of wicking geotextile was found to be useful in draining water from the soils in the pavement and reducing the risk of generating positive pore pressure that induces pumping. Three test sections on the shoulder of I-44 Highway in Missouri were constructed and instrumented. The construction of the field test section finished in September 2018. In total 33 water content reflectometers were placed in the three test sections. Two of these sections were treated by placing one layer of wicking geotextile on top of a clayey subgrade at the road shoulder. One control section without wicking geotextile was instrumented in order to make a comparison between improved and unimproved sections.

This report provides a summary of the initial report titled “PERFORMANCE OF WICKING GEOTEXTILE ON MITIGATING WATER PUMPING ISSUE ON I-44 HIGHWAY”. Additionally, the results of monitoring the field test section for more than 3 years from September 2018 to December 2021 are discussed in this report. Results obtained from field sections showed that the improvement in pavement drainage is considerable due to the installation of wicking geotextile.

Chapter. 1 Literature Review

This chapter provided a summary of the problem statement, limitations of current practice, and the proposed method to mitigate pumping in pavements. Additionally, the construction of the field test section is briefly presented.

1.1 Introduction

Pumping is caused by the migration of fines from subgrade soils into upper granular layers under the action of moving traffic [1]. It is one of the major factors contributing toward concrete pavement failures (Figure 1.1), which reduces the pavement life, affects road safety, and increases maintenance costs [2]. For pumping to occur, four basic conditions must exist: (1) A soil layer with a high amount of fines underlaying a granular layer having larger voids with no to little fines content, (2) soil that is saturated with free water, (3) repeated heavy axle loads that causes deflection of pavement and subsequently generates excess pore water pressure [3], and (4) presence of voids and cracks that form continuous paths to the road surface. Figure 1.1 shows the schematics of the pumping mechanism. Unfortunately, all four conditions are met in many pavement structures. Joints and cracks extensively exist in pavement structures. Rainwater can easily infiltrate and accumulate in pavement's larger voids and cracks. Under heavy axle loads, the deflection at these locations is also larger. Repeated heavy axle loads increase pore water pressure and over time, the "free" water, together with the fine materials, squeezes out through the continuous paths to the road surface. As the fine materials are pumped out, the voids of the pumping layer enlarge, and more "free" water is accumulated near the joints and cracks during rainfall events. In turn, more fine materials are pumped out and the pavement eventually fails due to lack of support. Therefore, if the amount of water (both "free" water and capillary water) held within the base course can be controlled at a relatively lower range (unsaturated condition), the fines within the base and subgrade will not be pumped out, and the overall pavement performance is expected to improve [4-6].

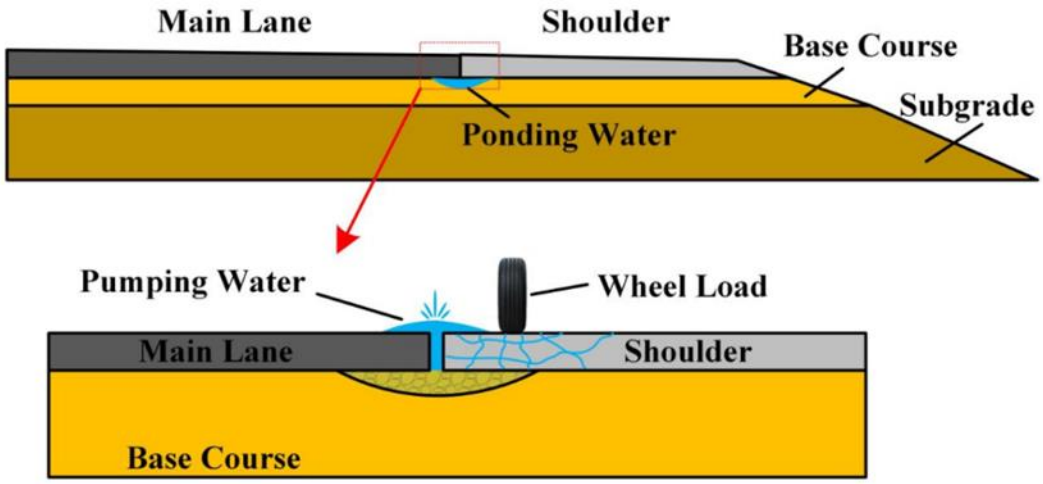

Figure 1.1 Schematics of pumping action.

In pavements, void space in form of joints, cracks, or voids between particles is always present. Consequently, removal of any of the other three conditions can mitigate or eliminate pumping, namely: a) limiting pavement deflection, b) separating fines from intruding upper layers, and c) removing free water by improving soil drainage. Numerous studies have been performed on the application of geotextiles in mitigating pumping in which the geotextiles were used as reinforcement [7-9], separation/filtration [10-19], and drainage [8]. The reinforcing effect of geotextile is mobilized by some degree of deflection under wheel load, and due to the low stiffness of most of the geotextiles, this function of geotextile has not gained popularity. Up to date, geotextile is mostly used as a separator/filter layer when it is used in pumping mitigation. However, issues such as clogging the drainage layer due to fines migration may occur [12]. Improving the drainage of the pavement system using geotextiles seems a promising and straightforward method in pumping mitigation. Pavement drainage is specifically important as repeated traffic load can drastically increase pore water pressure in the pavement, which accelerates the deterioration [20-25]. A major limitation of conventional geotextiles is their inability to drain capillary water since they can only drain free gravitational water under saturated conditions [27]. As a result, pavements having conventional geotextiles usually are under near-saturated to saturated conditions. Consequently, repeated traffic loads generate higher positive pore pressure under such conditions and potentially initiate pumping. It was reported that the cyclic wheel load can generate excess pore water pressure up to 28 kPa (4.1 psi) [3, 16]. Dempsey [26], based on field and experiment results, pointed out that a 20 kPa (2.9 psi) increase in pore pressure is enough to easily move finer grains (particles smaller than10 mm or 0.4 in.).

In recent years, a new type of wicking geotextile has been developed. Different from conventional geotextiles, the wicking geotextile was designed with polyethylene multifilament fibers for reinforcement and the specially designed nylon wicking fibers with deep grooves for lateral drainage purposes [26]. It was proven to be efficient in draining both free and capillary water under saturated and unsaturated conditions [29], and there have been several successful applications of the wicking geotextile due to this unique feature. Zhang and Presler, [30] first used the wicking geotextile to prevent frost heave and thaw weakening at Beaver Slide of the Dalton Highway in Alaska, and available data and field observations since 2010 have clearly indicated that the wicking geotextile has successfully eliminated the frost boil problem in the test section. Other examples included the Alaska Department of Transportation and Public Facilities' Dalton Highway 197-209 experimental feature project and Milepost 196 Parks Highway Broad Pass Railroad Overcrossing project [31-32]. In these projects, the wicking geotextile effectively removed the excess water in the pavement structure and improved pavement performance, leading to a significant cost saving on maintenance and repair [31]. In addition, field observations of the drainage performance of the wicking geotextile indicated that clogging was not a major issue, and the drainage system with the wicking geotextile still worked effectively in dehydrating road embankment 5 years after the completion of the project [32].

Figure 1.2a shows a picture of the wicking geotextile used in this study. The schematics of the cross-section of the wicking geotextile are illustrated in Figure 1.2b. As depicted in Figures 1.2a-b, the wicking geotextile has two different warp yarns which are weaved by wefts. The reinforcing warp yarn is made of polypropylene with high tensile strength. The unique properties of the wicking geotextile come from its wicking warps that are woven at the top, middle, and bottom of the fabric cross-section. These warps give the wicking geotextile a great potential for maximizing capillary action and water transport in an unsaturated environment. Each wicking warp consists of 144 hydrophilic and hygroscopic nylon wicking fibers (Figure 1.2c) for drainage purposes. These fibers are highly hydrophilic with multichannel cross-sections, which have a high shape factor and a great number of channels per fiber (specific surface area = 3650 cm2/g (16039 in.2/oz)). Each wicking fiber has an average diameter of 30-50 μm and the opening of the grooves is 5-12 μm (Figure 1.2c). The working mechanism of the wicking geotextile is depicted in Figure 1.2d. The weaving pattern of the wicking geotextile allows it to absorb water from both the top and the bottom sides and transport it along the deep grooved channels. Since the relative humidity of the air is usually less than 90% under most conditions, the suction caused by air at the surface of a pore is very high (>14 MPa or 2 ksi). If the end

of the wicking geotextile is exposed to the atmosphere, there is a high suction gradient in the wicking geotextile from its buried end in the soil to the exposed end. The suction gradient is the driving force that continuously transports water from the buried end of the wicking geotextile to the exposed end. Water is then vaporized into the surrounding atmosphere at the exposed end and gradually dries the soil.

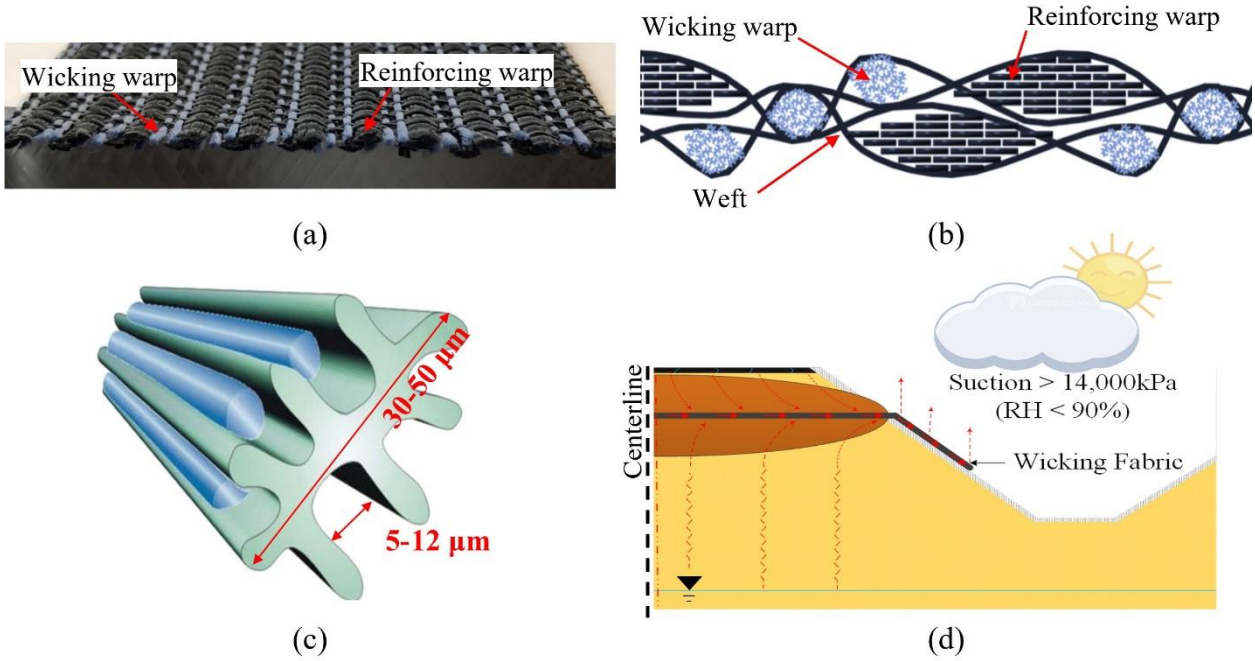

Figure 1.2 Wicking geotextile: a) fabric photo, b) schematics of fabric cross-section, c) schematics of a single fiber, and d) schematics of wicking geotextile working mechanism (adapted from [33]).

1.2 Construction of the Test Section

In order to evaluate the performance of the wicking geotextile, a full-scale field test section (Figure 1.3) was constructed and instrumented with the help of the Missouri Department of Transportation (MoDOT). A 225 ft. (68.6 m) -long road shoulder was selected at milepost 117.2 on the eastbound Interstate 44 in Missouri. Three sections, including a 30 ft. (9.1 m) -long control section, a 20 ft. (6.1 m)-long section 1, and a 175 ft. (53.3 m)-long section 2 were constructed (Figure 1.3a). The sections were instrumented with 33 water content reflectometers to measure volumetric water content (hereafter referred to as VWC) and temperature as shown by numbers in Figure 1.3a. For this type of sensor, the VWC measurement range is 0% to 100% ±3%, and the temperature measurement range is -50 to +70°C ±0.5°C (-58 to +158°F ±0.9°F) [35]. The control section was left untreated without the installation of the wicking geotextile. Section 1 was in the middle with the installation of a 15 ft. (4.6

m)-wide, toppled L-shape wicking geotextile at a depth 18 in. (46 cm) below the road surface at the interface of subgrade and the base course layer, as shown by a solid red line in figure 1.3a. In section 2, the 15 ft. (4.6 m)-wide wicking geotextile was placed horizontally at the interface of the subgrade and the base course layer at a depth 18 in. (46 cm) below the road surface.

Figures 1.3b shows the construction of the field test sections. The existing road shoulder was first excavated to a depth of 18 in. (46 cm) until the clayey subgrade was exposed. For each sensor installed within the subgrade layer, a hole was dug at a depth of 4 in. (10 cm) below the subgrade (22 in. (56 cm) below the final road surface) to place the sensor and then backfilled with uniform-graded sand. After installation of the sensors in the subgrade, the wicking geotextile was placed over the subgrade in sections 1 and 2. The second group of sensors was then installed right on top of the geotextile after its placement and covered with the sand (Figure 1.3b (left)). Due to the test sections' configuration, the outer edge of the wicking geotextile in section 2 was approximately 1 ft. (0.3 m) beyond that in section 1 as shown in Figures 1.3a and 1.3b. Next, a layer of base course material was placed in one lift and compacted above the subgrade (or the wicking geotextile) with the final height of 16 in. (41 cm) (Figure 1.3b (right)). The shallowest sensors in each section were then installed in the base course at a depth of 8 in. (20 cm) below the final road surface in a similar way as of the sensors in the subgrade. Finally, the base course was covered by a 2 in. (5 cm)-thick hot-mix asphalt (HMA). The construction of the field test sections was completed on September 28, 2018. The solid pink lines in Figure 1.3c show the vertical cross-section locations of the three test sections. Soil moisture and temperature in all test sections were monitored by the installed sensors right after the construction of test sections on September 28, 2018, at an interval of every 15 minutes. The results were then averaged into hourly readings and stored in the data logger for further analysis.

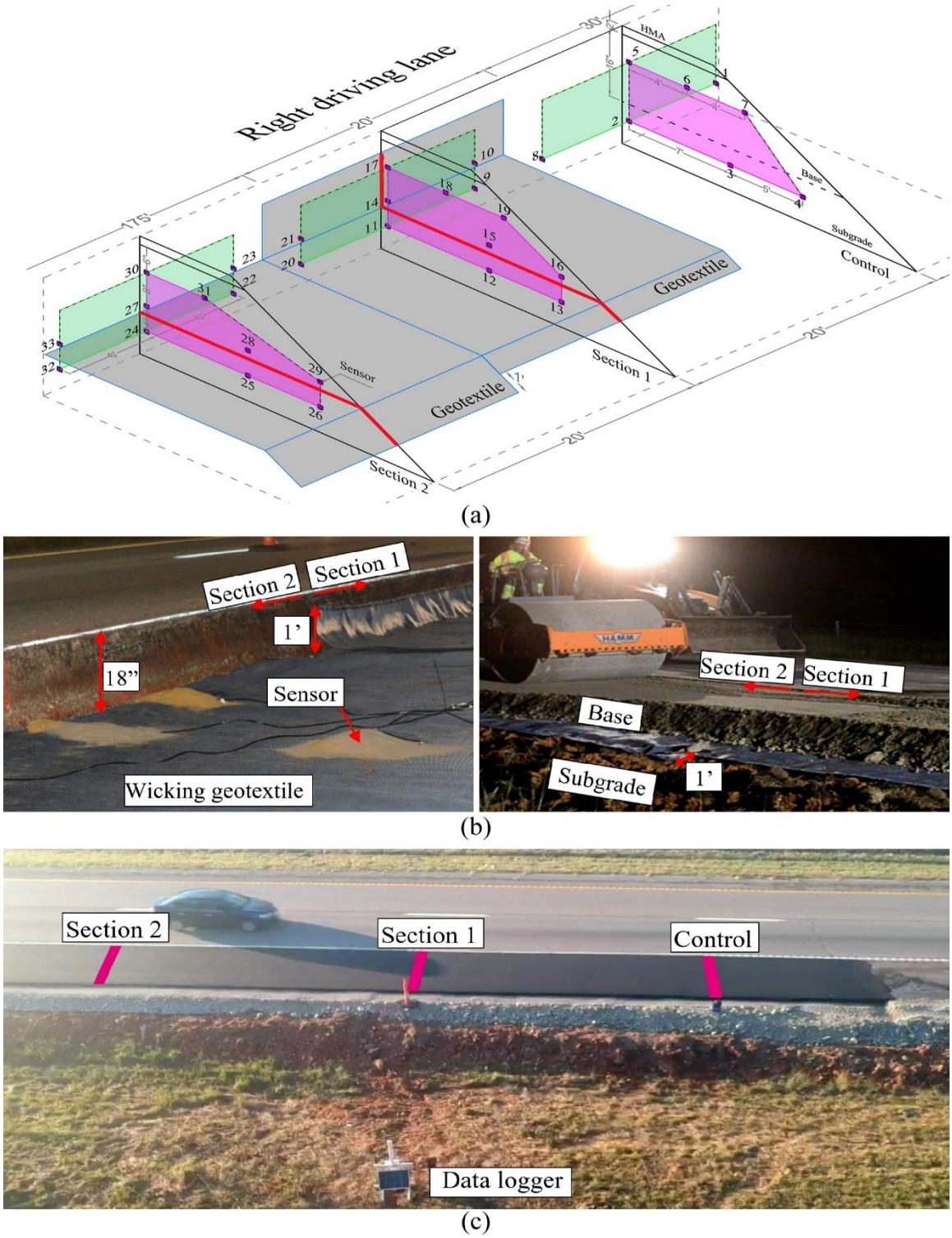

Figure 1.3 Field test sections. a) design schematics, b) installation of the wicking geotextile and the second layer of sensors (left), compaction of the base course (right), c) final configuration.

Chapter. 2 Local Climatic Data

Moisture content in the pavement structure is closely related to local climatic conditions. Hence, it is important to acquire local climatic data and compare it with the changes in moisture content in the pavement when analyzing the field data. Figure 2.1 shows the local climatic data obtained from the closest weather station (Camdenton, Missouri) 30 miles north of the field test section from 09/28/2018 to 12/23/2021.

As shown in Figure 2.1a, the mean daily air temperature varies between 20-30°C (68-86°F) in summer whereas in winter, air temperature fluctuates around (-5)-10°C (23-50°F) most of the time. This pattern repeats yearly without significant deviation from one year to another. The mean daily temperature in 102 days out of 1183 days was below the freezing temperature (0°C or 32°F).

Figure 2.1b shows the relative humidity during the monitoring period. The relative humidity ranged between 50-90% most of the time. It is clear that the air suction induced by the relative humidity (Figure 2.1c) was always greater than 1 MPa (145 psi), with an overall average of around 100 MPa (14.5 ksi). This suction generates a hydraulic gradient in the wicking geotextile that is the driving force that continuously transports water from the buried end to the exposed end of the wicking geotextile.

Precipitation indicates how much water is available to infiltrate into the pavement system. As shown in Figure 2.1d, precipitation was observed in 356 days out of 1183 days, with an accumulative value of 3005 mm (118 in.). Each year, most of the precipitation occurred from April to July, mainly in the form of rain. The total amount of precipitation is divided into infiltration, runoff, and evaporation. Usually, rainfall infiltration is the main cause of the increase in soil moisture.

Potential evapotranspiration in Figure 2.1d represents the maximum ability of a certain climatic condition to vaporize water from a free water surface. Although the actual evapotranspiration could be different from the potential evapotranspiration due to the availability of water in the pavement system and other factors, the potential evapotranspiration is a good indication of the amount of water that could be lost from a surface. The daily potential evapotranspiration, calculated based on ASCE's standardized reference evapotranspiration equation [36], is presented in Figure 2.1d with the cumulative value of 2869 mm (113 in.). As explained before, water that is transported to the exposed end of the wicking geotextile is vaporized continuously and causes the soil around the wicking geotextile to gradually dry.

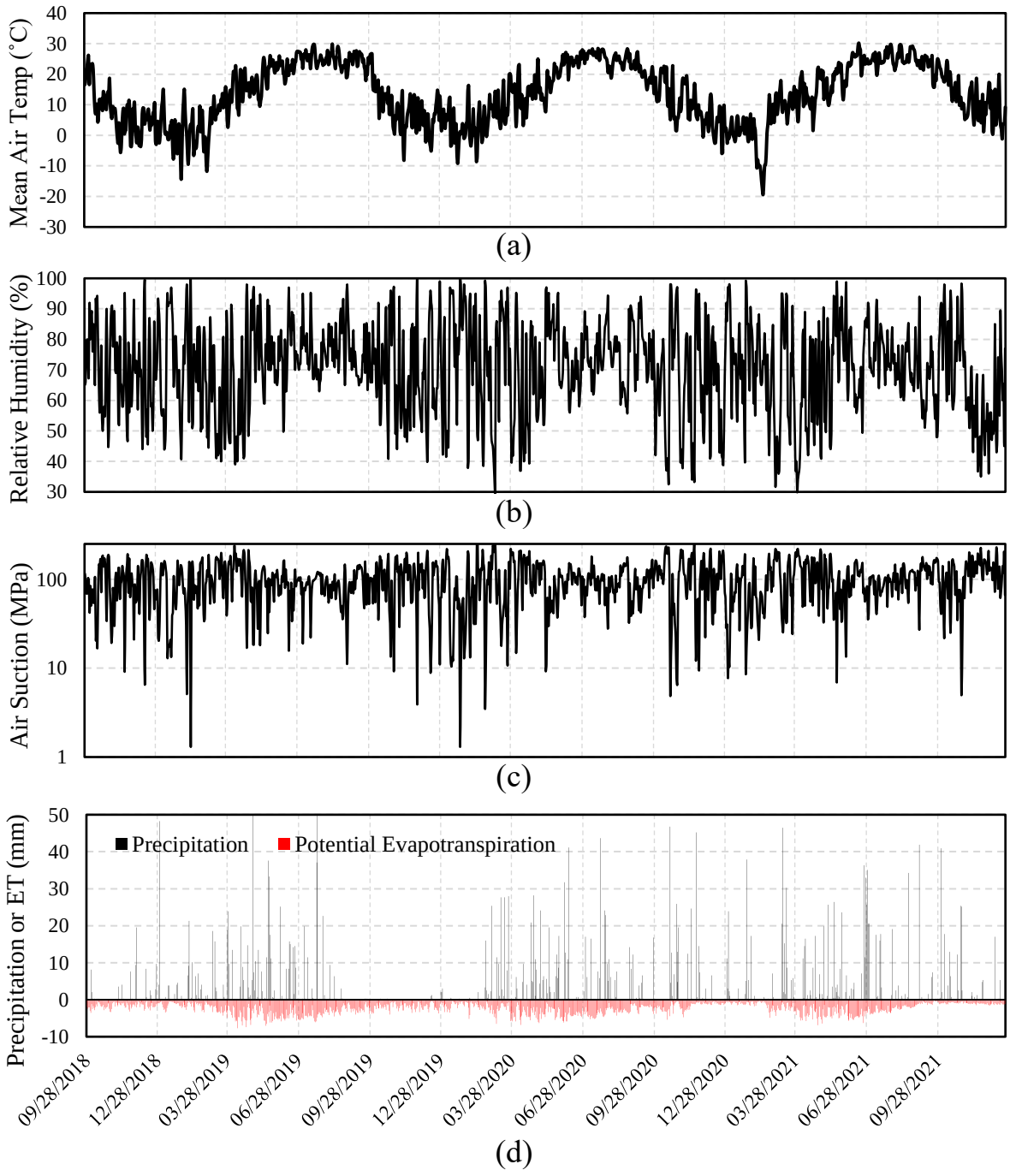

Figure 2.1 Average daily climatic data. a) Mean air temperature, b) Relative humidity, c) Air suction, d) Precipitation and potential evapotranspiration.

Chapter. 3 Performance of the Test Section

In this chapter, the performance of the field test section is discussed. First, general observations and maintenance on the test section are presented. Later, temperature and moisture data obtained from the field test section is used to evaluate and discuss the performance of the field test section.

3.1 General Fieldwork

Throughout the monitoring period, quarterly routine visits to the field test section were made. During each visit, visual observations were made on the situation of the test section. In addition, sensors' data was collected to be used to evaluate the subgrade/base layer situation. Additional trips were made as necessary in order to resolve issues that were encountered during the monitoring period. Detailed information on these issues is provided in the following paragraphs.

As mentioned in the preliminary report, the whole width of the wicking geotextiles in sections 1 and 2 was completely covered by the base course layer when the construction of the field test section was completed. Later, on 2/9/2019 soils at the shoulders of test sections, 1 and 2 were removed to expose the wicking geotextile to air to facilitate the drainage (Figure 3.1). The exposed length of the wicking geotextile in sections 1 and 2 was at least 12 in. along the whole length of the corresponding sections. During a visit on 9/13/2020, it was found that the wicking geotextile in test section 1 was completely covered by the collapsed base course soils and grass, while in test section 2, most of the wicking geotextile was covered. 10 days later on 9/23/200, an additional trip was made to the field test section. In this trip, the collapsed soils and grass were removed to expose the wicking geotextiles in both sections 1 and 2 (Figure 3.2).

(a) (b)

Figure 3.1 Field test section situation on 2/9/2019. a) before exposing the end of the wicking geotextile, and b) after exposing the end of the wicking geotextile.

(a (b)

Figure 3.2 Field test section situation. a) Field test section situation on 9/13/2020 before exposing the end of the wicking geotextile, and b) Field test section situation on 9/23/2020 after exposing the end of the wicking geotextile.

Figure 3.3 Ant nests inside the datalogger chamber.

3.2 Soil Temperature Data

In the following paragraphs results of temperature measurements at different locations in the test section are discussed.

Figure 3.4 shows the temperature variation in sensors 5, 17, 30, located at depth 8 in. below the shoulder surface in the control section, section 1, and section 2, respectively. It can be seen that the temperature variations in different years are very consistent. In summer, the temperature rose to around 35°C (95°F) and it dropped to around 5°C (41°F) during wintertime. Except for a short period in early 2021, the base layer did not experience subfreezing temperature. Noting that these sensors are located near the top of the base layer, soil freezing is unlikely to occur in the field test section.

As mentioned before, Ants nesting caused some data loss between 5/5/200-9/23/2020. During this period the data related to some of the sensors, like sensor 30, was not recorded. This period is shown by the green dashed double arrow in Figure 3.4. In addition, sensor 5 shows false temperature readings for the most part in 2021. This problem might have been caused by mechanical damage or other unpredicted issues.

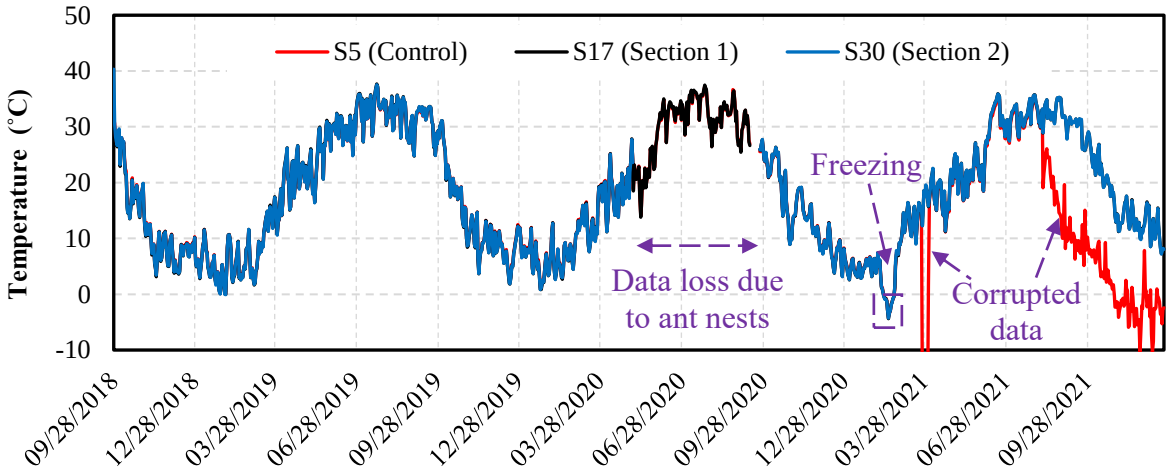

Figure 3.4 Temperature variation near the top of the base layer in the control section.

Similar to sensor 5, sensors 10, 13, 22, and 28 have also stopped working at some time during the monitoring period. The temperature readings in these sensors have been removed from the analyzed data. The time at which each of these sensors stopped working is displayed in Figure 3.5. The arrows in Figure 3.5 show the time when each sensor stopped reading valid temperature. Since most of the sensors stopped working is within a few months before the data loss as a result of ant nests, it is believed that

ants inside the datalogger chamber might have caused electrical short-circuit in these sensors and caused permanent damage to them. It should be noted that the permanent damage mainly affected the temperature measurement circuit in these sensors. As it will be shown later, the soil moisture measurement of these sensors was used in the analysis despite their false temperature measurements.

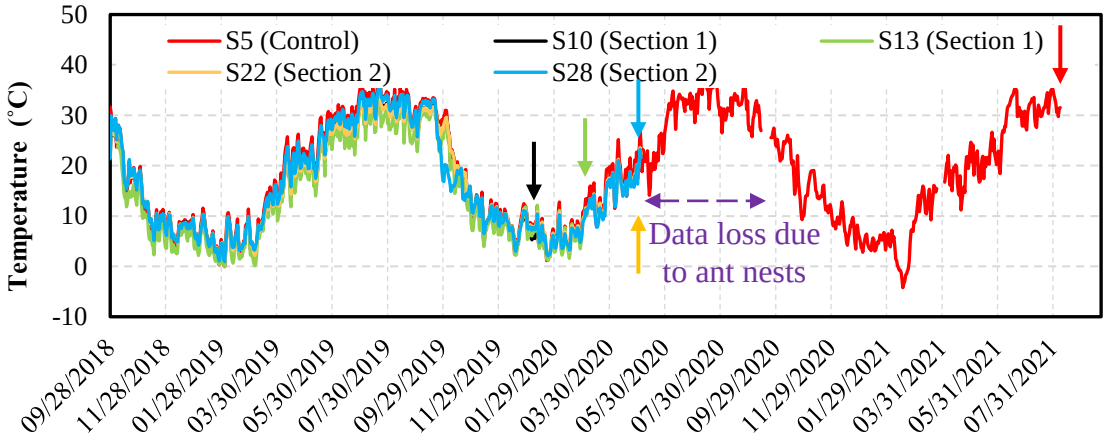

Figure 3.5 Temperature variation in corrupted sensors.

Since the temperature in other locations in the base layer and the subgrade was very similar to what has been presented in Figure 3.4, the soil temperature is not discussed further.

3.3 Soil Moisture Data

The main objective of this chapter is to analyze soil moisture data in the test section, in order to evaluate its performance with regards to the pumping issue.

The VWC profiles over the entire monitoring period at different locations of road shoulder are shown in Figure 3.6 (using results from several sensors as examples). The VWC data in section 2 from May 2020 to October 2020 was missing due to the ant nesting issue, as indicated by the discontinued VWC for section 2 in Figure 3.6. Therefore, it was assumed that the trend of the VWC during the discontinued period was close to that of the previous year. Figure 3.6a shows the variation of VWC from the sensors at the inner edge of the base course in the control section (sensor 5), section 1 (sensor 17), and section 2 (sensor 30). Over the entire monitoring period, the VWCs at all sections were always higher than the VWC at which the base layer was compacted. As a result, pavement performance was never as good as that at the end of the construction. After the initial increase in VWC and the following drop, the VWC in the soil was almost constant for nearly three months. The VWC of section 1 was the highest with a value of around 0.37. The VWC of the control section was approximately 0.35. The

moisture in section 2 however, was much less than the other sections and the VWC was around 0.29, as a result of longer exposed end.

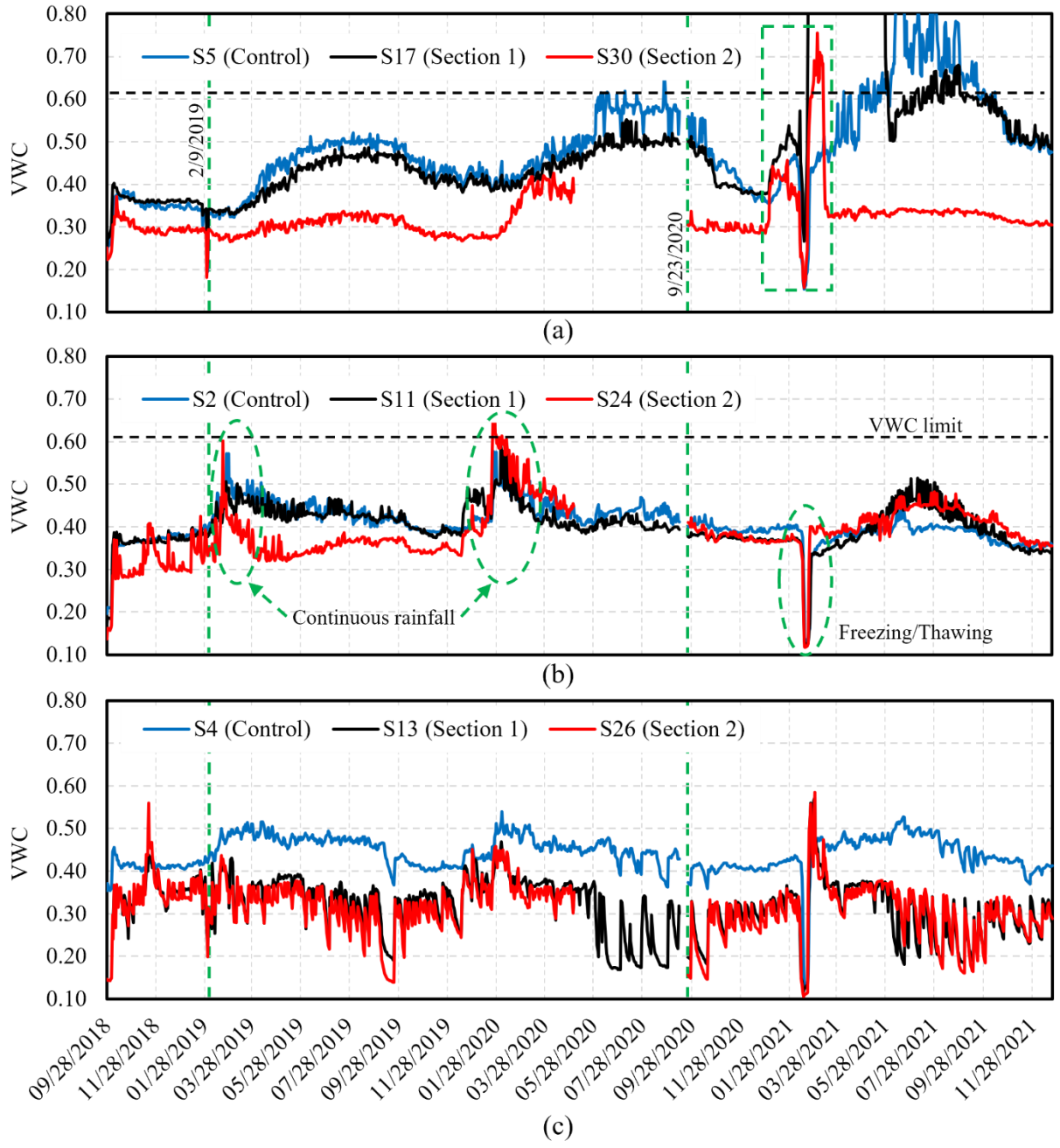

Figure 3.6 VWC profiles at different locations of the road shoulder. a) near the top of the base course close to the vertical interface of the right driving lane and the road shoulder, b) near the top of the subgrade close to the vertical interface of the right driving lane and the road shoulder, c) in the subgrade below the wicking geotextile close to side slope.

As mentioned earlier, the outer end of the wicking geotextile was exposed to the atmosphere on

2/9/2019 and 9/23/2020, as indicated by vertical dashed green lines in Figure 3.6. It can be seen from Figure 3.6a that the trend of the VWC profiles in sections 1 and 2 changed right after exposing the end of the wicking geotextile. Over a period of approximately 10 days, the VWC reduced by approximately 0.01 and 0.03 in sections 1 and 2, respectively. As the exposed area of the geotextile surface increased, it's expected that the evaporation rate from its surface increased, and thus the suction on the outer end of the wicking geotextile increased, and more water was reduced from the soil. By March 2019, with an increase in the precipitation, the VWC in all sections increased gradually until the end of July 2019. During these four months where the VWC was relatively high, the average increase in VWC in the control section, sections 1 and 2 were 0.16, 0.11, and 0.05, respectively. As can be seen in Figure 3.6a, the increase in VWC in section 2 was the least. In addition, before exposing the end of the wicking geotextile on 2/9/2019, the VWC in section 1 was higher than the control section. However, after exposure, the VWC increase in section 1 dropped below the control section. By April 2019, the VWC in section 1 was well below that of the control section, indicating the improved drainage performance of the wicking geotextile since a longer width of wicking geotextile was exposed to the atmosphere. From October 2019, the VWCs in all sections started to reduce due to less precipitation and then increased from February 2020 due to the increase in precipitation. By April 2020, the VWC in section 2 started to reduce despite the increases in VWC in other sections. Please note that the evapotranspiration at this time, as shown in Figure 3.6c, is the highest in 2020. As a result, the soil in section 2 dried quickly. At the beginning of 2021, a sudden increase in VWC corresponding to a few days of high intensity of rainfall was observed, followed by a quick drop due to freezing, and then another sudden increase in VWC due to the thawing process as shown by a dashed green rectangle. In both rainfall and thawing time in this period, the increase in moisture in section 2 occurred quicker than in other sections. This was because the extra moisture added by successive heavy rainfalls or thawing may have flowed back into the pavement as the exposed portion of the wicking geotextile became nearly saturated. At this time, the soil inside the pavement was still under unsaturated condition. The hydraulic gradient vector was then from the exposed edge of the wicking geotextile to the inside of the pavement, transporting water into the pavement.

Another reason for the apparent increase in moisture content after the thawing is the infiltration of saltwater into the soil. Road salt applied during winter has possibly dissolved in water and percolated into the soil and caused an increase in the electrical conductivity of the soil bulk. Since the VWC in the soil is measured using the electrical conductivity of the soil, the added salt to the soil increased the

electrical conductivity measured by the sensor. The sensors used in this study can measure VWC accurately if the electrical conductivity measurement is less than 0.9 ds/m (deci-siemens per meter). Assuming the soil void ratio is constant over the monitoring period, the limiting electrical conductivity measurement corresponds to VWC equal to a value around 0.61. As a result, any VWC reading beyond 0.61 is a result of soil bulk electrical conductivity of higher than 0.9 ds/m. The black horizontal dashed line in Figures 3.6a-b shows the limiting valid VWC measurement (0.61) for the sensor used in this study. Nonetheless, quickly after the exposed end of the geotextile was dried, soil moisture started to be wicked out of the pavement.

The VWC profiles at the inner end of the shoulder in the subgrade below the wicking geotextile in the control section (sensor 2), and sections 1 (sensor 11) and 2 (sensor 24) are shown in Figure 3.6b. One of the main differences of the VWC variations in Figure 3.6b compared to what has been shown in Figure 3.6a, was the sharper increase in VWC variations during rainfalls. This can be explained by the distance of the sensors from the wicking geotextile. As the sensors were placed closer to the wicking geotextile, the water that was transported from the nearly saturated exposed end of the geotextile reached the sensors quicker. This means that the difference in VWC in dry and wet conditions would be larger and the transition time between these extremes would be shorter. Similar to the VWC variations in the base layer (Figure 3.6a), the VWC in the subgrade showed the superior performance of the sections with wicking geotextile. In general, the VWC in section 2 was up to 0.11 less than that of the control section. Wicking geotextile in section 1 with shorter exposed length, reduced moisture from the soil up to 0.03 compared to the control section. During a few heavy and/or continuous rainfalls and thawing as shown by green dashed ovals in Figure 3.6b, the VWC in sections 1 and 2 were higher than the control section for a short period of time. However, quickly after the runoff water was removed from the surface of the geotextile, the VWC dropped quickly in the soil due to the wicking process.

Figure 3.6c shows the variation of VWC in the clayey subgrade, at the outer edge of the subgrade below the wicking geotextile in the control section (sensor 4), section 1 (sensor 13), and section 2 (sensor 26), respectively. These sensors were installed near the side slope of the road shoulder where the subsurface flow regime was highly affected by the sloped boundary. In general, the difference in VWC right before and after any rainfall event was higher in this location. Individual rainfall events can be easily identified from the spikes in the graphs of sections 1 and 2. In these sections where wicking geotextile was installed, water quickly drained out after the rainfall was over. On the other

hand, the overall VWC in the control section was much higher than those in sections 1 and 2 most of the time. As can be observed in Figure 3.6c, the fluctuation of VWC in the control section was much less than those in sections 1 and 2. The reason for this is that in the control section, due to lower drainage performance, water accumulated by the recurring rainfalls. Since the water could not drain as fast as other sections, the control section showed less fluctuation amplitude of VWC during rainfalls, indicating that the overall permeability of the section was relatively low. The low permeability delayed the increase in the water content during the rainfall the same way as it prevented the soil from draining water quickly.

It is important to point out that pumping usually occurs at the interface between the driving lane and the shoulder. Thus, reducing the water content at this location is crucial for pumping mitigation. Signs of pumping were abundant at this location as well as similar locations along the shoulder prior to the construction of the test section. As observed in Figures 3.6a-b, the VWC in this location was reduced up to 5-15% in spring when the pavement was relatively wetter than in other seasons. If it is assumed that the control section at its wettest condition was saturated, then, section 1 and especially section 2 were far from saturated conditions with negative pore-water pressures. As pumping is induced by positive pore pressure build-up [35], the improved section showed much less likelihood of pumping.

To better understand the effect of installing the wicking geotextile in reducing water content in the paved shoulder, the spatial distribution of the VWC was plotted at moments of before, during, and after a specific rainfall, as shown in Figure 3.7. Figure 3.7a shows the distribution of VWC on 11/12/2018, which is 7 days before the rainfall of 11/19/2018. At least one week had passed since the last rainfall and all test sections were relatively dry. Section 2 was the driest among all sections. The driest location in section 2 is at the upper part of the interface between the driving lane and the shoulder, which indicated superior performance since if the soil at that point were dry, it is unlikely for the pumping to occur.

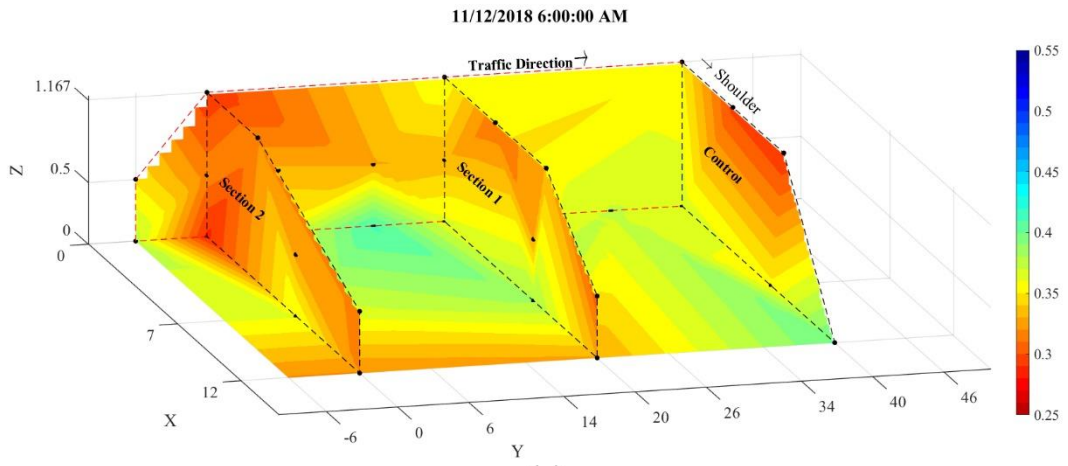
11/12/2018 6:00:00 AM
Traffic Direction
Shoulder
Control
Section 1
Section 2
Z
1.167
0.5
0
X
0
7
12
Y
-6
0
6
14
20
26
34
40
46
0.55
0.5
0.45
0.4
0.35
0.3
0.25

(a)

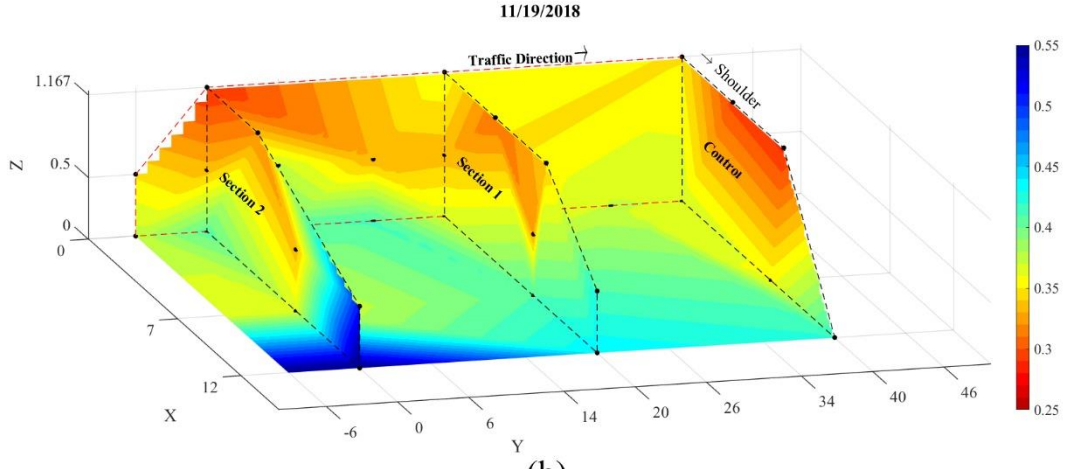
11/19/2018
Traffic Direction
Shoulder
Control
Section 1
Section 2
Z
1.167
0.5
0
X
0
7
12
Y
-6
0
6
14
20
26
34
40
46
0.55
0.5
0.45
0.4
0.35
0.3
0.25

(b)

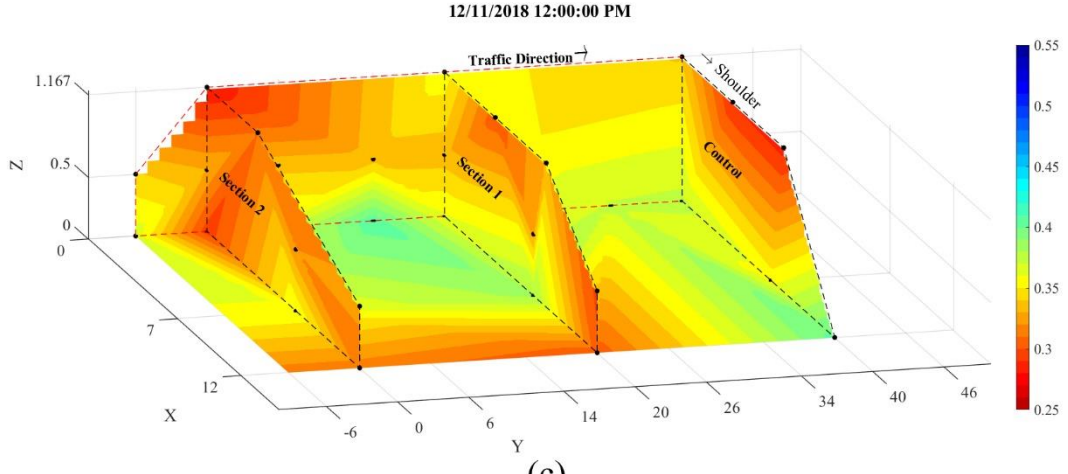
12/11/2018 12:00:00 PM
Traffic Direction
Shoulder
Control
Section 1
Section 2
Z
1.167
0.5
0
X
0
7
12
Y
-6
0
6
14
20
26
34
40
46
0.55
0.5
0.45
0.4
0.35
0.3
0.25

(c)

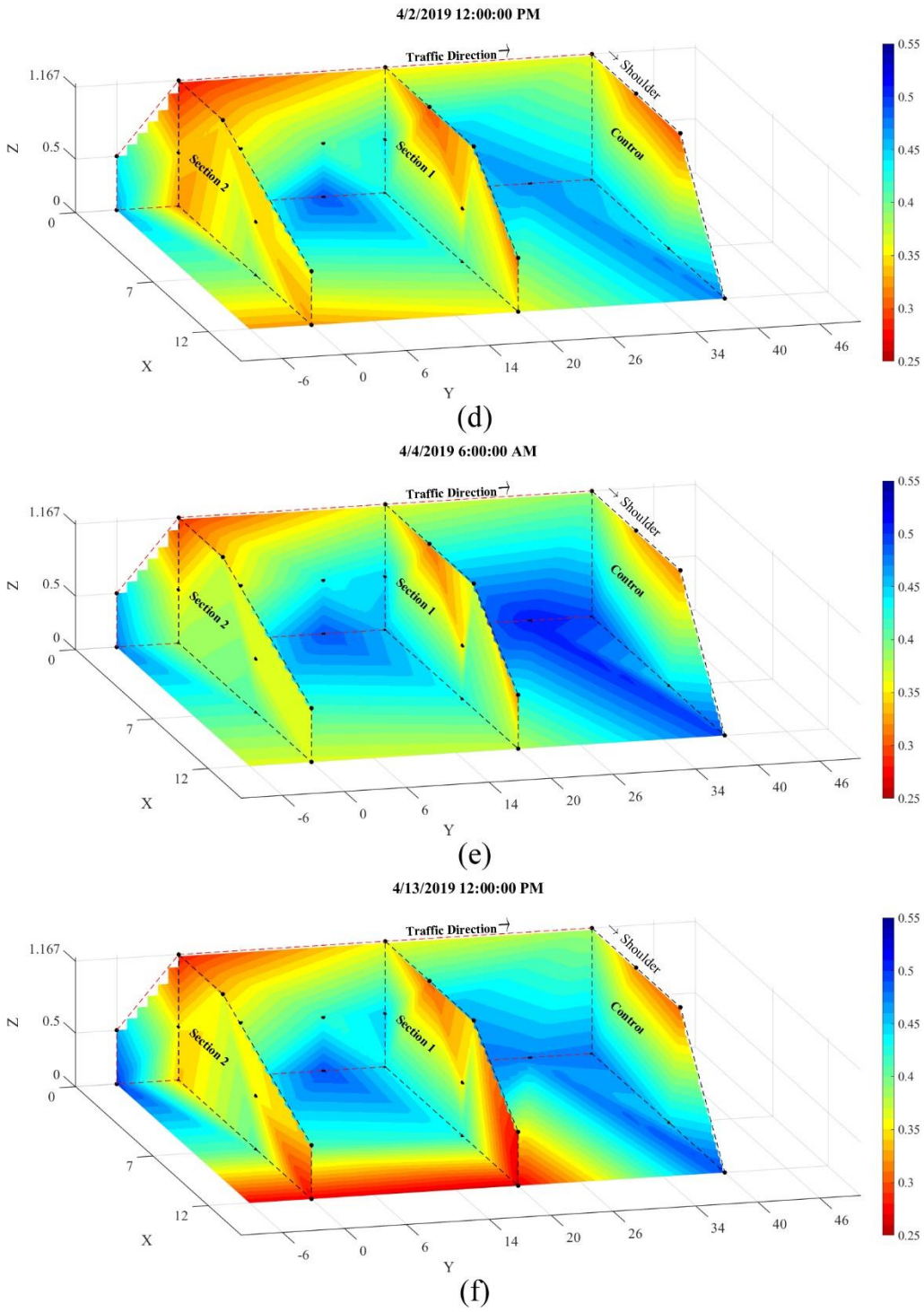

Figure 3.7 VWC at different times before exposing the tip of the wicking geotextile at section 1. a) before rainfall on 11/12/2018, b) during rainfall on 11/19/2018, c) after rainfall on 12/11/2018, and after exposing the tip of the wicking geotextile at section 1: d) before rainfall on 4/2/2019, e) during rainfall on 4/4/2019, f) after rainfall on 4/13/2019.

Figure 3.7b shows the spatial distribution of the VWC during a rainfall event of 11/19/2018. The VWCs in all three sections increased in general, although the increases at the side slope portion were larger than that inside the shoulder. In addition, a noticeable increase in VWC at the inner edge of section 2 was observed. The VWC change in section 1 was between the increase in control and section 2. Figure 3.7c shows the distribution of VWCs in all sections after one week of no rainfall. Compared with Figure 3.7b, it was found that larger changes in VWC occurred in soils near the surface than those inside the road shoulder, and the largest VWC changes occurred in section 2 at the lower part of the interface between the driving lane and the shoulder. At similar locations in section 1, there were no visible changes in VWC, while in the control section, there was a slight increase in the VWC. Note that these readings took place before exposing the edge of the wicking geotextile.

A comparison of the same phenomenon after exposing the edge of the wicking geotextile in section 1 is shown in Figures 3.7d through 3.7f. Figure 3.7d shows the distribution of VWC on 4/2/2019, a few days after the last rainfall when the pavement was relatively dry. The overall VWC was higher than that shown in Figure 3.7a, indicating that the VWC increased during the spring of 2019. Section 2 was the driest section and section 1 was drier than the control section. During the rainfall on 4/4/2019 (Figure 3.7e), the VWC increased in all sections. The increase in VWC in subgrade at the inner edge of the pavement was much more compared to the upper layers. After eight days (Figure 3.7f), sections 1 and 2 noticeably dried compared to the control section, specifically at the outer edge of the pavement. Similar to what has been observed in Figures 3.7a through 9c, the superior performance of the improved sections is obvious.

Chapter. 4 Conclusions

In this study, a new type of wicking geotextile was used to mitigate pumping in pavements in Missouri. A field test section was constructed at milepost 117.2 of eastbound Interstate 44 in Missouri. In order to compare the different placements of the wicking geotextile in reducing moisture content in the pavement, three sections were designed. One was the control section without wicking geotextile, section 1 was a section with L-shaped wicking geotextile, and section 2 was a section with the horizontal installation of wicking geotextile. Continuous monitoring of these sections from September 2018 to December 2021 clearly demonstrated that the installation of wicking geotextile had considerably reduced the moisture content in the pavements structure and was beneficial to the mitigation of the pumping issue, especially where the pavement is prone to pumping damage. The key findings of this study are summarized as follows:

1. Although the road shoulder was constructed at very low initial moisture content, the moisture content in the road shoulder quickly increased to a high level after the first rainfall and never dropped to the initial moisture content. As a result, pavement performance was never as good as that at the end of the construction.

2. Moisture contents in all three test sections in the road shoulder constantly changed with the local climatic conditions. Rainfall infiltration was the major reason for moisture content increase, which occurred quickly after the beginning of each rainfall event. Even though there were no signs of surface damage/crack on the shoulder up to the time of this report, a considerable amount of water was infiltrated into the pavement's subsurface layers.

3. Installation of a layer of wicking geotextile successfully drained more water from the pavement and provided a drier subgrade/base course layer.

4. Exposing the end of the wicking geotextile increased its drainage performance noticeably. To obtain the best performance, the end of the wicking geotextile needs to remain exposed to the atmosphere.

5. During rainfalls, water could backflow into the pavement from the exposed end of the wicking geotextile for a short period. However, shortly after rainfall stopped, wicking

geotextile drains water out of the soil.

6. Among all three test sections, section 2 with the horizontal installation of wicking geotextile performed the best due to the longer exposed length. Section 1 installed with L-shaped wicking geotextile performed much better than the control section.

7. The reduction in VWC near the top of the base course layer was up to 25% in section 2 where a horizontal layer of wicking geotextile was installed. On average, the VWC in section 2 was around 10% less than the control section at the top of the base course layer where the pumping damage was mostly observed prior to the construction of the test section.

Although this study did not directly address the separation/filtration functions of the wicking geotextile regarding the pumping issue, it has been shown that the wicking geotextile successfully drained capillary water in pavements and increased average suction in soil. The reduction in average soil moisture at least delays the pumping if not completely prevent it. This would be beneficial in mitigating pumping since even under repeated traffic load, the pore water pressure would not reach positive values, thus, the potential pumping and clogging would not occur.

It's noted that all the discussions presented in this report were based on the results from a limited monitoring time period (39 months). As pumping is a gradual process that takes place over a long time, continued monitoring of field sections is strongly recommended for a better understanding of the effect of wicking geotextile on long-term pavement performance.

References

[1]. Huang YH. Pavement Analysis and Design. 2nd ed. Pearson Education. Pearson/Prentice Hall; 2004. 775 p.

[2]. Bhatti MA, Barlow JA, Stoner JW. Modeling damage to rigid pavements caused by subgrade pumping. Journal of Transportation Engineering. 1996;122(1):12–21.

[3]. Alobaidi I, Hoare DJ. The development of pore water pressure at the subgrade-subbase interface of a highway pavement and its effect on pumping of fines. Geotextiles and Geomembranes. 1996 Feb 1;14(2):111–35.

[4]. Kandhal PS, Lubold CW, Roberts FL. Water damage to asphalt overlays: Case histories. National Center for Asphalt Technology Nashville, Tennessee; 1989.

[5]. Christopher BR, Schwartz CW, Boudreau RL. Geotechnical aspects of pavements: Reference manual. US Department of Transportation, Federal Highway Administration; 2010.

[6]. Duong TV, Cui Y-J, Tang AM, Dupla J-C, Canou J, Calon N, et al. Physical model for studying the migration of fine particles in the railway substructure. Geotechnical Testing Journal. 2014;37(5):895–906.

[7]. Abu-Farsakh M, Hanandeh S, Mohammad L, Chen Q. Performance of geosynthetic reinforced/stabilized paved roads built over soft soil under cyclic plate loads. Geotextiles and Geomembranes. 2016 Dec 1;44(6):845–53.

[8]. Han J. Design of Planar Geosynthetic-Improved Unpaved and Paved Roads. In: Pavement and Geotechnical Engineering for Transportation. Reston, VA: American Society of Civil Engineers; 2013. p. 31–41.

[9]. Hufenus R, Rueegger R, Banjac R, Mayor P, Springman SM, Brönnimann R. Full-scale field tests on geosynthetic reinforced unpaved roads on soft subgrade. Geotextiles and Geomembranes. 2006 Feb 1;24(1):21–37.

[10]. Ayres DJ. Geotextiles or geomembranes in track? British railways' experience. Geotextiles and Geomembranes. 1986 Jan 1;3(2–3):129–42.

[11]. Black PJ, Holtz RD. Performance of Geotextile Separators Five Years after Installation. Journal of Geotechnical and Geoenvironmental Engineering. 2002 May;125(5):404–12.

[12]. Chapuis RP, Contant A, Baass KA. Migration of fines in 0-20 mm crushed base during

placement, compaction, and seepage under laboratory conditions. Canadian Geotechnical Journal. 2008 Mar 25;33(1):168–76.

[13]. Collins BM, Mahoney JP, Holtz RD. FWD Analysis of Pavement Sections with Geotextile Separators. In: Advances in Pavement Engineering. Reston, VA: American Society of Civil Engineers; 2005. p. 1–14.

[14]. DeBerardino SJ, Baldwin JS. West Virginia Department of Transportation's use of a free-draining base and the role of geotextiles as long-term separators. Geotextiles and Geomembranes. 1996 Mar 1;14(3–4):187–92.

[15]. Grau HR. Engineering Criteria for Use Of Geotextile Fabrics In Pavement And Railroad Construction. Army Engineer Waterways Experiment Station Vicksburg Ms Geotechnical Lab; 1984.

[16]. Huang J, Su Q, Wang W, Wang X, Guo H. Vibration behavior and reinforcement effect analysis of the slab track-subgrade with mud pumping under cyclic dynamic loading: Full-scale model tests. Shock and Vibration. 2018 Sep 13;2018:1–14.

[17]. Loulizi A, Al-Qadi IL, Bhutta SA, Flintsch GW. Evaluation of Geosynthetics Used as Separators. Transportation Research Record: Journal of the Transportation Research Board. 2007 Jan 18;1687(1):104–11.

[18]. Snaith MS, Bell AL. The filtration behaviour of construction fabrics under conditions of dynamic loading. Geotechnique. 1978 Dec 25;28(4):466–8.

[19]. Yang C, Yu X. Mud-pumping prevention of railway subgrade by using geotextile. In: Proceedings of the Tenth International Conference on Soil Mechanics and Foundation Engineering. 1989. p. 1693–5.

[20]. Alobaidi I, Hoare DJ. Qualitative criteria for anti-pumping geocomposites. Geotextiles and Geomembranes. 1998 Aug 1;16(4):221–45.

[21]. Alobaidi I, Hoare D. Factors affecting the pumping of fines at the subgrade subbase interface of highway pavements: A laboratory study. Geosynthetics International. 1994;1(2):221–59.

[22]. Trani LDO, Indraratna B. Assessment of Subballast Filtration under Cyclic Loading. Journal of Geotechnical and Geoenvironmental Engineering. 2010 Nov;136(11):1519–28.

[23]. Miszkowska A, Lenart S, Koda E. Changes of Permeability of Nonwoven Geotextiles due to Clogging and Cyclic Water Flow in Laboratory Conditions. Water. 2017 Sep 1;9(9):660.

[24]. Kermani B, Xiao M, Stoffels SM. Analytical study on quantifying the magnitude and rate of

subgrade fines migration into subbase under flexible pavement. Transportation Geotechnics. 2019 Mar 1;18:46–56.

[25]. Kermani B, Xiao M, Stoffels SM, Qiu T. Reduction of subgrade fines migration into subbase of flexible pavement using geotextile. Geotextiles and Geomembranes. 2018 Aug 1;46(4):377–83.

[26]. Dempsey BJ. Laboratory and field studies of channeling and pumping. Transportation Research Record. 1982;849:1–12.

[27]. Lin C, Galinmoghadam J, Han J, Liu J, Zhang X. Quantifying and Incorporating the Benefits of Wicking Geotextile into Pavement Design. Journal of Transportation Engineering, Part B: Pavements. 2021 Jul 8;147(3):04021044.

[28]. Lin C, Zhang X, Han J. Comprehensive Material Characterizations of Pavement Structure Installed with Wicking Fabrics. Journal of Materials in Civil Engineering. 2018 Feb;31(2):04018372.

[29]. Lin C, Zhang X. A bio-wicking system to dehydrate road embankment. Journal of Cleaner Production. 2018 Sep 20;196:902–15.

[30]. Zhang X, Presler W. Use of H2Ri Wicking Fabric to Prevent Frost Boils in the Dalton Highway Beaver Slide Area, Alaska. Alaska University Transportation Center, Alaska Department of Transportation and Public Facilities; 2012.

[31]. Currey J. H2Ri Wicking Fabric Experimental Feature Final Report Dalton Highway MP 197-209 Rehabilitation. Technical report, Alaska DOT&PF, Project No. IM-DP-065- 4(8)/61214. 2016.

[32]. Lin C, Presler W, Zhang X, Jones D, Odgers B. Long-Term Performance of Wicking Fabric in Alaskan Pavements. Journal of Performance of Constructed Facilities. 2016 Apr;31(2):D4016005.

[33]. Lin C, Zhang X, Galinmoghadam J, Guo Y. Advances of a New Wicking Geotextile with Lateral Drainage Capabilities in Roadway Applications. In: Transportation Research Board 98th Annual MeetingTransportation Research Board. Washington, D.C.; 2019.

[34]. Galinmoghadam J, Zhang X. Use of Wicking Fabric to Reduce Pavement Pumping. In: GeoCongress 2020. Minneapolis, MN: American Society of Civil Engineers; 2020. p. 630–9.

[35]. Zhang X, Galinmoghadam J. Performance of Wicking Geotextile on Mitigating Water Pumping Issue on I-44 Highway. 2020.

[36]. Walter IA, Allen RG, Elliott R, Jensen ME, Itenfisu D, Mecham B, et al. ASCE's standardized reference evapotranspiration equation. In: Watershed management and operations management 2000. 2000. p. 1–11.